Experimental constant beamwidth transducer

A. L. Van Buren, L. Dwight Luker, M. D. Jevnager, and A. C. Tims
Naval Research Laboratory, Underwater Sound Reference Detachment, P.O. Box 8337, Orlando, Florida 32856

(Received 26 October 1982; accepted for publication 11 February 1983)

The theory of a broadband constant beamwidth transducer (CBT) which is based on Legendre function shading of a spherical cap was described in a previous report [P. H. Rogers and A. L. Van Buren, J. Acoust. Soc. Am. **64**, 38–43 (1978)]. Theoretical calculations showed the CBT to have uniform acoustic loading, extremely low side lobes, virtually no nearfield, an essentially constant beam pattern for all frequencies above a certain cutoff frequency, and a flat transmitting current response over a broadband for piezoelectric drive. In this paper we present experimental results obtained for a prototype CBT based on fifth-order Legendre function shading. The transducer is a spherical cap with a diameter of 30.5 cm and a total cap angle of 50°. Measurements on the CBT showed it to possess very low side lobes and a nearly constant beamwidth over the frequency range from 20 to 140 kHz for ambient pressures up to 3.4 MPa. We also present formulas useful in the design of a CBT which is to be used as a transmitter and/or receiver. The formulas involve simple algebraic and trigonometric expressions which can be readily evaluated using a pocket calculator.

PACS numbers: 43.88.Ar, 43.30.Yj, 43.30.Jx, 43.20.Px

INTRODUCTION

Most directional acoustic transducers and arrays exhibit beam patterns which are frequency dependent. Thus, the spectral content of the transmitted or received signal varies with position in the beam, and the fidelity of an underwater acoustic system depends on the relative orientation of the transmitter and receiver. In a previous paper[1] we described a simple method for obtaining a transducer whose beamwidth is essentially independent of frequency over a broad bandwidth. Our constant beamwidth transducer (CBT) is a rigid spherical cap of arbitrary half-angle α shaded so that the normal velocity on the outer surface is proportional to $P_\nu(\cos\theta)$, where P_ν is the Legendre function whose root of smallest angle occurs at $\theta=\alpha$. That is, the normal velocity is a maximum at the center of the cap at $\theta=0$ and decreases according to $P_\nu(\cos\theta)$ until it is zero at $\theta=\alpha$. For every choice of α there is a corresponding choice for ν, the order of the Legendre function. The required value for ν is not, in general, an integer.

Theoretical calculations show that the CBT has uniform acoustic loading, extremely low side lobes, and an essentially constant beam pattern for all frequencies above a certain cutoff frequency. Under piezoelectric drive the transducer has a flat transmitting current response over a broadband. In addition, the CBT has virtually no nearfield; i.e., the acoustic pressure distribution (with respect to θ) is essentially the same at all radial distances from near the transducer surface to the farfield. The surface pressure distribution as well as the pressure distribution out to the farfield is approximately equal to the surface velocity distribution.

Although the previous paper[1] emphasized the transmitter aspects of the CBT, the concept is equally applicable to receivers. The concept is also applicable to an acoustically transparent spherical cap. In fact, Trott[2] has applied the results presented in an earlier unpublished version of Ref. 1 to the theoretical design of a receiver CBT using $P_1(\cos\theta)=\cos\theta$ shading on an acoustically transparent hemispherical cap. However, the beam pattern from such a CBT is bidirectional, containing a backlobe identical to the frontlobe.

In this paper we describe the experimental confirmation of the CBT concept. We present results obtained for a prototype CBT based on fifth-order Legendre function shading. We also present formulas useful in the design of a CBT which is to be used as a transmitter and/or receiver. The formulas involve simple algebraic and trigonometric expressions which can be readily evaluated using a pocket calculator. They are based on excellent approximations for the Legendre functions of noninteger order, and thus avoid the need for evaluating these rarely encountered functions. We obtain formulas for the required velocity distribution, cutoff frequency, directivity index, equivalent two-way beamwidths for volume and surface reverberation, and spherical cap size. The formulas are presented in Sec. I. Design considerations are discussed in Sec. II. Included are shading coefficients for a CBT with a stepwise implementation of the Legendre function shading distribution. The prototype CBT is described in Sec. III. Results of measurements on the prototype are given in Sec. IV. Last, Sec. V contains the summary and conclusions.

I. THEORY

A. Velocity distribution

The key to the special properties of the CBT is its surface normal velocity distribution $u(\theta)$ given by

$$u(\theta)=P_\nu(\cos\theta),\quad 0<\theta<\alpha_\nu,$$
$$u(\theta)=0,\quad \theta>\alpha_\nu, \tag{1}$$

where α_ν is the zero of smallest angle of the Legendre function $P_\nu(\cos\theta)$. We showed in Ref. 1 that the CBT need not extend beyond α_ν, and thus can be constructed as a spherical cap whose half-angle is equal to α_ν. Consequently, we call α_ν the cap half-angle, although in practice the actual cap half-angle for a P_ν CBT can possess any value $\theta>\alpha_\nu$. The order ν of the Legendre function can be chosen to be any real num-

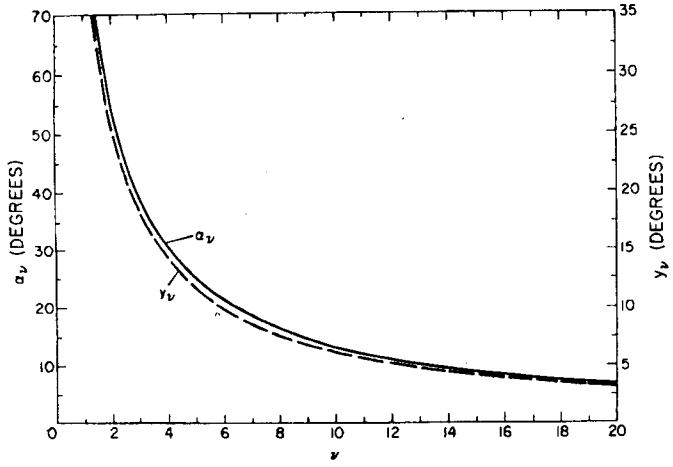

FIG. 1. Variation of the cap half-angle α_ν and the -3-dB half-angle γ_ν as a function of the Legendre function order ν.

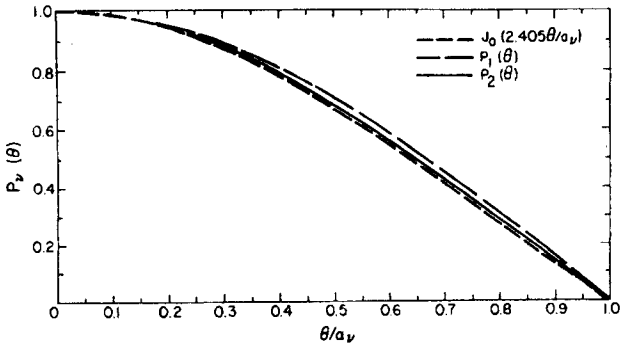

FIG. 3. Comparison of $P_\nu(\cos\theta)$ and $J_0(2.4048\theta/\alpha_\nu)$ as a function of θ/α_ν for $\nu = 1$ and 2.

ber greater than zero. The corresponding angle α_ν decreases monotonically from near 180° as ν increases from just above zero. However, in order to obtain the reasonably simple design formulas presented in this paper, we restrict ν to be equal to or greater than unity. This simultaneously restricts α_ν to be equal to or less than 90°. We do not expect this restriction to be of any consequence since there do not appear to be many (if any) sonar applications calling for a CBT with α_ν greater than 90°. If such applications do occur, then design formulas corresponding to, but more complicated than, those given in this paper can be obtained for $\nu < 1$. The following approximation for α_ν, in degrees,

$$\alpha_\nu \simeq \frac{137.796}{(\nu+0.5)}\left(1-\frac{0.045}{(\nu+0.5)^2}\right), \tag{2}$$

is correct to within 0.03% for $\nu \geqslant 1$. We present in Fig. 1 a graph of α_ν as a function of ν. We also include a graph of the -3-dB half-angle γ_ν; i.e., the value for θ such that $P_\nu^2(\cos\theta) = 0.5$. The following approximation for γ_ν, in degrees,

$$\gamma_\nu \simeq \frac{64.540}{(\nu+0.5)}\left(1+\frac{0.103}{(\nu+0.5)^2}\right), \tag{3}$$

is believed to be correct to within 0.1% for $\nu \geqslant 1$.

The Legendre function $P_\nu(\cos\theta)$ is a monotonically decreasing function of θ in the range $0 \leqslant \theta \leqslant \alpha_\nu$. In Fig. 2 we show $P_\nu(\cos\theta)$ over this range for $\nu = 5$, 7.5, and 10. The function $P_\nu(\cos\theta)$ can be evaluated to any desired accuracy by use of its hypergeometric expansion in $(1-\cos\theta)/2$. Fortunately, use of this expansion is unnecessary for our purposes. Sufficiently accurate values over the range $0 \leqslant \theta \leqslant \alpha_\nu$ can be obtained using the following excellent approximation in terms of the zeroth order cylindrical Bessel function of the first kind:

$$P_\nu(\cos\theta) \simeq [\pi\theta/(180\sin\theta)]^{1/2} J_0(2.4048\theta/\alpha_\nu), \tag{4}$$

with both θ and α_ν given in degrees. For $\nu = 1$, the error in Eq. (4) is less than 0.1% for $0 \leqslant \theta \leqslant 35°$, less than 0.2% for $35° < \theta \leqslant 55°$, and less than 0.4% over the remainder of the range $55° < \theta \leqslant 90°$. The error decreases rapidly with increasing ν.

For large values of ν, the range of θ is small and the factor $[(\pi\theta/(180\sin\theta)]^{1/2}$ approaches unity and can be discarded. Thus for large ν, we obtain the simple approximation

$$P_\nu(\cos\theta) \simeq J_0(2.4048\theta/\alpha_\nu). \tag{5}$$

Graphs of $P_\nu(\cos\theta)$ and $J_0(2.4048\theta/\alpha_\nu)$ as a function of θ/α_ν are shown in Fig. 3 for $\nu = 1$ and 2. The agreement between $J_0(2.4048\theta/\alpha_\nu)$ and $P_\nu(\cos\theta)$ for $0 \leqslant \theta \leqslant \alpha_\nu$ improves rapidly with increasing ν, being reasonably good at $\nu = 1$ and very good for $\nu = 2$. Graphs of the closer approximation given by Eq. (4) for $\nu = 1$ and 2 would be indistinguishable from the curves shown in Fig. 3 for $P_1(\cos\theta)$ and $P_2(\cos\theta)$, respectively. Accurate numerical values for the Bessel function $J_0(x)$ can either be calculated using the polynomial approximations given in Abramowitz and Stegun[3] or obtained from tables such as those given in Refs. 4 and 5.

We obtain from Eq. (4) with $\nu = 1$:

$$P_1(\cos\theta) = \cos\theta \simeq [\pi\theta/(180\sin\theta)]^{1/2} J_0(2.4048\theta/90), \tag{6}$$

for $0 \leqslant \theta \leqslant \alpha_1 = 90°$. We can invert this equation to provide

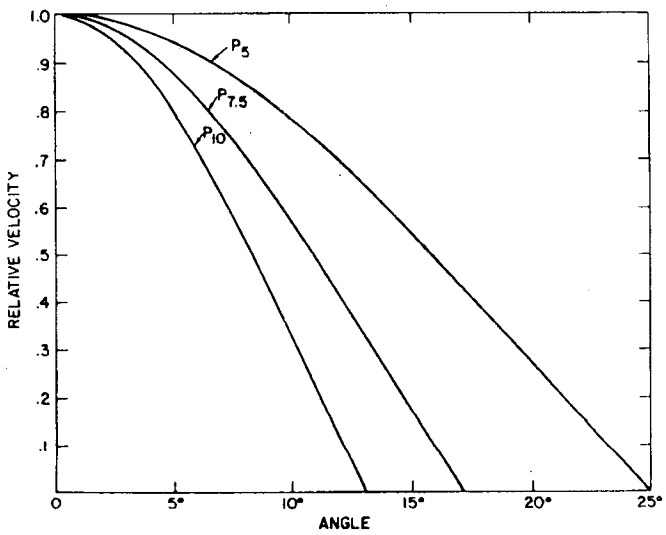

FIG. 2. Velocity shading functions of a P_5 CBT, a $P_{7.5}$ CBT, and a P_{10} CBT.

the following approximation for $J_0(x)$:

$$J_0(x) \simeq \left(\frac{\sin(90x/2.4048)}{\pi x/4.8096}\right)^{1/2} \cos\left(\frac{90x}{2.4048}\right), \tag{7}$$

where the arguments of both sin and cos are in degrees. The relative error in this approximation increases monotonically from 0% to a maximum of almost 0.4% as x increases from zero to just below the first root of $J_0(x)$ at $x = 2.4048$. As x increases from just above the first root to a value near π, the relative error decreases monotonically from nearly 0.4% to less than 0.01%. Beyond $x = \pi$, the relative error increases rapidly, being 0.4% at $x = 3.35$ and 4.7% at $x = 4.0$.

We can substitute J_0 from Eq. (7) into Eq. (4) to obtain the following approximation for $P_\nu(\cos\theta)$, $0 \leqslant \theta \leqslant \alpha_\nu$, in terms of trigonometric functions:

$$P_\nu(\cos\theta) \simeq \left(\frac{\sin(90\theta/\alpha_\nu)}{(90/\alpha_\nu)\sin\theta}\right)^{1/2} \cos\left(\frac{90\theta}{\alpha_\nu}\right), \tag{8}$$

where again the arguments of sin and cos are in degrees. Because of the nature of its derivation, this approximation is exact for $\nu = 1$. For $\nu > 1$ and $0 < \theta < \alpha_\nu$, the approximation is always somewhat larger than $P_\nu(\cos\theta)$. The relative error for all $\nu > 1$ increases as θ approaches α_ν and reaches a maximum of less than 0.4% for values of θ just less than α_ν. We believe that the approximation given in Eq. (8) is quite adequate for most purposes in designing a CBT.

B. Beam patterns and cutoff frequency

The beam pattern $g(\theta)$ of a P_ν CBT, i.e., a CBT shaded according to P_ν, approaches the square of the normal velocity distribution in the limit of high frequency. Thus, the limiting pattern is rotationally symmetrical, has a maximum in the direction of the axis of the spherical cap, decreases monotonically to zero at the cap half-angle α_ν, and is equal to zero for $\theta \geqslant \alpha_\nu$. Approximations for both the pattern null α_ν and the -3-dB half-angle y_ν in terms of ν were given as Eqs. (2) and (3), respectively, in the last section. Approximations of the velocity distribution given by Eqs. (4), (5), and (8) are also appropriate for describing the limiting beam patterns.

As the frequency decreases from high to low values, the CBT beam patterns tend to resemble the high-frequency limit less and less. The highest frequency below which the resemblance is less than acceptable is called the low-frequency cutoff f_c. A general rule of thumb for the cutoff frequency f_c in kHz is given by

$$f_c = c[1.10 + (24.6/y_\nu)]/(1500b), \tag{9a}$$

where c is the sound speed of the surrounding fluid in m/s, b is the half-arclength (i.e., radius) of the spherical cap in meters, and y_ν is in degrees. This rule of thumb is equivalent to the one given in Ref. 1 in terms of kb, where k is the wavenumber. By use of Eqs. (2) and (3) we can alternately express f_c in terms of the cap half-angle α_ν in degrees by

$$f_c \simeq c\frac{1.10 + (52.5/\alpha_\nu)(1 - 7.79\times10^{-6}\alpha_\nu^2)}{1500b}, \tag{9b}$$

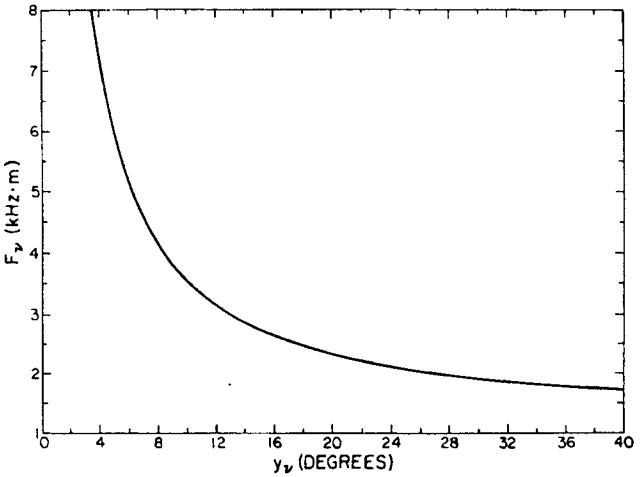

FIG. 4. Frequency constant F_ν in kHz·m as a function of the -3-dB half-angle y_ν in degrees.

or, in terms of the Legendre function order ν by

$$f_c \simeq c\frac{1.10 + 0.381(\nu + 0.5)[1 - 0.103/(\nu + 0.5)^2]}{1500b}. \tag{9c}$$

If a is the radius of curvature of the cap, then $b = \pi a\alpha_\nu/180$.

Since Eqs. (9a) to (9c) are only general rules of thumb, we use a value of 1500 m/s for the sound speed c when calculating f_c for a CBT to be used in water, even though the actual sound speed of the water might be somewhat different than this. The cutoff frequency f_c and the inverse of the cap radius scale together. We define as the frequency constant for a CBT radiating into water the quantity $F_\nu = f_c b = 1.10 + (24.6/y_\nu)$. A graph of the behavior of the frequency constant F_ν as a function of the -3-dB half-angle y_ν is shown in Fig. 4. We note that the definition for f_c given above differs slightly for low ν from that given in Ref. 1. The difference is only 1.4% at $\nu = 1$ and decreases rapidly with increasing ν.

The choice of the frequency below which the beam patterns are unacceptable is a subjective one and depends strongly on the applications that the user has in mind for the CBT. As an example, we show in Fig. 5 calculated beam patterns for a $P_{2.75}$ CBT. The -3-dB half-angle for $P_{2.75}$ is 20°. The beam pattern at $10f_c$ is indistinguishable from the $P_{2.75}$ velocity distribution. The beam pattern at $3f_c$ for angles less than about 32° is nearly identical with that at $10f_c$, however, the two patterns differ somewhat for larger angles. The same is true for $2f_c$, although the deviation from the $10f_c$ beam pattern for $\theta > 32°$ is greater. As the frequency is decreased below $2f_c$, we begin to see a significant deviation from the $10f_c$ beam pattern for $\theta \geqslant 32°$. The deviation for angles above 32° appears to increase monotonically with decreasing frequency, however, the deviation below 32° is greater at $1.2f_c$ than at f_c or $0.8f_c$. Examination of the extrema curves presented in Ref. 1 for P_5, $P_{7.5}$, and P_{10} CBT's suggests that the portion of the beam pattern around the -10-dB angle changes less with frequency than any other part of the pattern. Thus, if we are primarily concerned with the constancy of the beam pattern for angles less than

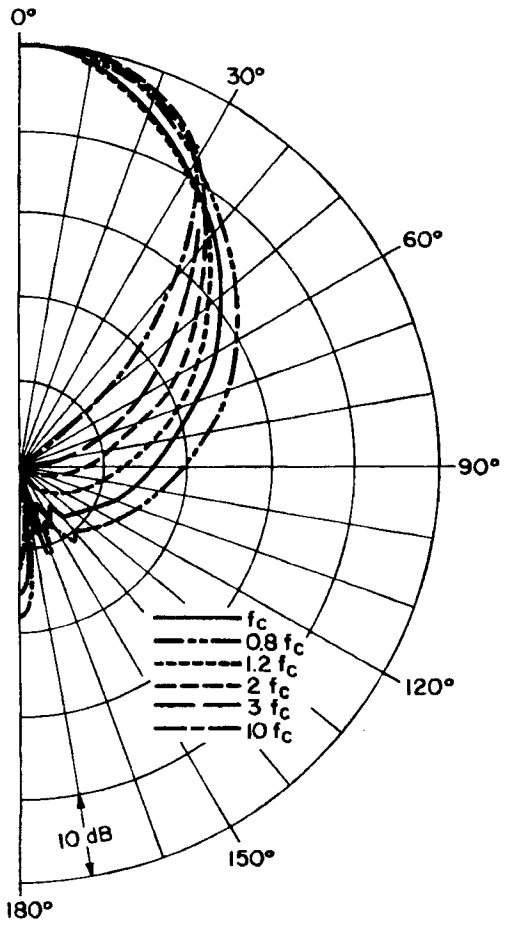

FIG. 5. Calculated beam patterns for a $P_{2.75}$ CBT at selected relative frequencies f/f_c.

the -10-dB angle, and only require that there be no substantial side lobes for higher angles, then the cutoff frequency for $P_{2.75}$ can be chosen as low as $0.8f_c$. On the other hand, if constancy of the beam pattern for larger angles is required, then the cutoff frequency must be chosen somewhat larger than f_c.

Additional information on the theoretical variation of the CBT beam patterns with frequency is provided in Ref. 1. There the calculated range of beam patterns is given for a P_5 CBT, a $P_{7.5}$ CBT, and a P_{10} CBT, both for frequencies above the cutoff frequency f_c and for frequencies above $2f_c$.

C. Directivity index

The directivity index DI for a CBT is given by

$$\mathrm{DI} = -10\log_{10}\left(\frac{1}{2}\int_0^{\pi\alpha_\nu/180} P_\nu^2(\cos\theta)\sin\theta\,d\theta\right). \tag{10}$$

Rewriting Eq. (4) so that θ is in radians, substituting the resulting expression for $P_\nu(\cos\theta)$ into Eq. (10), and integrating exactly, we obtain the approximation

$$\mathrm{DI} \simeq -20\log_{10}\alpha_\nu + 46.88, \tag{11a}$$

with α_ν in degrees.

We can alternatively express the result in terms of ν by use of Eq. (2) to give

$$\mathrm{DI} \simeq 20\log_{10}(\nu+0.5) + 4.09 + [0.391/(\nu+0.5)^2]. \tag{11b}$$

Equations (3) and (11b) can then be used to obtain the corresponding expressions for DI in terms of the -3-dB half-angle y_ν in degrees:

$$\mathrm{DI} \simeq -20\log_{10} y_\nu + 40.29 + 3.09\times10^{-4} y_\nu^2. \tag{11c}$$

All three approximations are accurate to within 0.1 dB for $\nu = 1$, and increase rapidly in accuracy with increasing ν.

D. Volume reverberation

Volume reverberation is characterized by an equivalent two-way beamwidth. The integral expression for this quantity[6] is

$$\psi = \int_0^{2\pi}\int_0^{\pi} b(\theta,\phi)\,b'(\theta,\phi)\sin\theta\,d\theta\,d\phi, \tag{12}$$

where $b(\theta,\phi)$ and $b'(\theta,\phi)$ are the beam patterns of the projector and receiver, respectively, and (θ,ϕ) are the standard spherical angles with the z axis being the principle direction of radiation. For the case where $b(\theta,\phi) = b'(\theta,\phi) = P_\nu^2(\cos\theta)$, we have

$$\psi = 2\pi\int_0^{\pi\alpha_\nu/180} P_\nu^4(\cos\theta)\sin\theta\,d\theta. \tag{13}$$

We rewrite the approximation for $P_\nu(\cos\theta)$ given in Eq. (5) so that θ is in radians and substitute in Eq. (13). Replacing $\sin\theta$ by θ, expanding $J_0(z)$ in the first three terms of its power series, multiplying out $J_0^4(x)$, integrating the result term by term, and adding a correction term necessary for low ν, we obtain

$$\psi \simeq 0.000147\alpha_\nu^2(1 + 6.84\times10^{-6}\alpha_\nu^2), \tag{14}$$

where α_ν is in degrees. We can also express this in terms of the -3-dB half-angle y_ν in degrees:

$$\psi \simeq 0.00067\, y_\nu^2(1 - 3.65\times10^{-5} y_\nu^2), \tag{15}$$

or, expressed in dB,

$$10\log_{10}\psi \simeq 20\log_{10} y_\nu - 31.7 - 1.59\times10^{-4} y_\nu^2. \tag{16}$$

This result is nearly identical to that for a circular plane array (circular piston) in an infinite rigid baffle. A similar result of a polar cap on a sphere acting as a circular piston was reported earlier by Butler and Ehrlich.[7] The inaccuracy in the approximations given in Eqs. (14) and (15) is less than 1%, while that of Eq. (16) is less an 0.1 dB.

E. Surface reverberation

Surface reverberation is characterized by a corresponding two-way beamwidth Φ given by the integral expression[6]

$$\Phi = \int_0^{2\pi} b(0,\phi)\,b'(0,\phi)\,d\phi. \tag{17}$$

For a P_ν CBT projector and receiver:

$$\Phi = 2\int_0^{\pi\alpha_\nu/180} P_\nu^4(\cos\theta)\,d\theta. \tag{18}$$

Use of the procedure described above in the previous section for obtaining Eq. (14) leads to the following approximation

for Φ, accurate to within 1%:

$$\Phi \simeq 0.0123\alpha_\nu(1 + 7.93\times 10^{-6}\alpha_\nu^2), \tag{19}$$

with α_ν in degrees. We can alternatively express Φ in dB accurate to within 0.1 dB in terms of the -3-dB half-angle y_ν in degrees:

$$10\log_{10}\Phi \simeq 10\log_{10} y_\nu - 15.8 - 9.77\times 10^{-5} y_\nu^2. \tag{20}$$

This result is about 3 dB lower than the value quoted for the circular plane array by Urick[6] in his Table 8.1. However, a close inspection of the problem reveals that Urick's values for $10\log_{10}\Phi$ for the circular plane array, the rectangular array, and the horizontal line are all in error by 3 dB. This is probably due to a factor of 2 error in the transcription by Urick of previous results expressed in terms of a surface reverberation index J_s. This surface reverberation index was defined to be $J_s = 10\log_{10}(\Phi/2\pi)$, as opposed to the volume reverberation index $J_v = 10\log_{10}(\psi/4\pi)$.

Evaluation of the surface reverberation for nonzero values of θ is more difficult than for $\theta = 0$. Simple expressions are not likely to exist for this case. Numerical integration appears necessary for each desired value for θ and ν. However, the simplest case of $\nu = 1$ can be solved analytically and yields

$$\Phi(\theta = \theta_0) = \cos^4\theta_0 \Phi(\theta = 0), \tag{21}$$

or

$$\Phi(\theta_0) = P_1^4(\cos\theta_0)\Phi(0), \tag{22}$$

or, in dB,

$$10\log_{10}\Phi(\theta_0) = 10\log_{10}\Phi(0) + 40\log_{10} P_1(\cos\theta_0). \tag{22a}$$

Based on this result, we might expect that the more general expression

$$10\log_{10}\Phi(\theta_0) = 10\log_{10}\Phi(0) + 40\log_{10} P_\nu(\cos\theta_0) \tag{23}$$

is a good approximation for small values of θ_0.

F. Spherical cap size

As stated earlier, the special radiation properties of the CBT result from the presence of a normal velocity distribution over the outer surface of a spherical cap given by $u(\theta) = P_\nu(\cos\theta)$ for $0 \le \theta \le \alpha_\nu$ and $u(\theta) = 0$ for $\theta > \alpha_\nu$. The cap half-angle must be at least as large as α_ν; to minimize the size and weight of the CBT we choose the cap half-angle equal to α_ν. A cross-sectional view of the spherical cap for a P_5 CBT is shown in Fig. 6.

In order to determine the radius b of the spherical cap (i.e., the half-arclength, not to be confused with the radius of curvature a of the cap) required for a CBT, we need first to specify the desired beam pattern. Typical choices for specifying the beam pattern are α_ν or the -3-dB half-angle y_ν. The order ν of the Legendre function shading corresponding to y_ν or α_ν can be calculated using the following approximations (accurate to within 0.1% for $\alpha_\nu < 90°$ and $y_\nu < 45°$):

$$\nu \simeq (64.540/y_\nu)(1 + 2.26\times 10^{-5} y_\nu^2) - 0.5 \tag{24a}$$

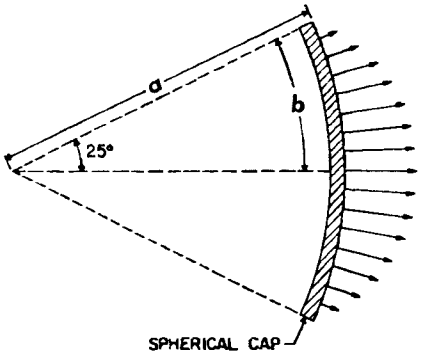

FIG. 6. Cross-sectional view of the spherical cap for a P_5 CBT. Arrows indicate the relative surface velocity distribution. The cap radius b is measured on the outer spherical surface.

and

$$\nu \simeq (137.796/\alpha_\nu)(1 - 2.43\times 10^{-6}\alpha_\nu^2) - 0.5. \tag{24b}$$

We must next specify the lowest desired operating frequency f_c of the CBT. We can now calculate the required cap radius in meters by use of

$$b = c[1.10 + (24.6/y_\nu)]/(1500 f_c), \tag{25a}$$

or

$$b \simeq c\frac{1.10 + (52.5/\alpha_\nu)(1 - 7.79\times 10^{-6}\alpha_\nu^2)}{1500 f_c}, \tag{25b}$$

where the sound speed c of the surrounding fluid is in m/s, f_c is in kHz, and y_ν and α_ν are in degrees.

II. DESIGN CONSIDERATIONS

The most obvious choice for the transduction material in the CBT for underwater applications is a piezoelectric ceramic such as lead zirconate–titanate. Experimental results show that it is difficult if not impossible to control the velocity distribution over a spherical cap consisting entirely of a single piece of piezoelectric ceramic. The presence of a variety of mechanical vibration modes in the ceramic cap produces a velocity distribution that is highly frequency dependent. We can avoid this problem by subdividing the ceramic cap into small pieces. We choose the lateral dimensions of each individual ceramic piece small enough so that there are no lateral vibration modes in the frequency band of operation that are sufficiently excited to significantly affect the normal velocity of the piece. We also choose the thickness of the ceramic pieces so that the lowest thickness mechanical resonance occurs well above the maximum operating frequency. The resulting mosaic can be attached to a backing plate that is mechanically rigid enough to maintain the shape of the spherical surface under operating conditions.

It is desirable to mechanically and acoustically isolate the ceramic from the backing plate by a thin layer of decoupling or pressure-release material such as corprene. This prevents the backing plate from vibrating and producing undesired acoustic radiation in the backward ($\theta \simeq 180°$) direction. It also prevents the normal velocity distribution from being adversely affected by mechanical resonances that might oth-

erwise be excited in the backing plate. We can also eliminate undesired acoustic radiation from the edges of the piezoceramic pieces by covering them with small strips of corprene.

We believe that corprene can be used as a decoupling material to a water depth of about 340 m without incurring significant changes in performance of the CBT. When the water depth is greater than about 340 m, however, the corprene is substantially compressed by the ambient water pressure and becomes too stiff to be effective in decoupling the ceramic from the backing plate. If the required water depth is too great for a pressure-release material to be successful in decoupling the ceramic from the backing plate, the backing plate probably must be made nearly acoustically rigid in order to prevent substantial acoustic radiation in the backward direction. In this case, the backing plate can no longer be lightweight but must be made of material with a large mass density-sound speed product such as steel or tungsten.

The inner and outer surfaces of the ceramic pieces are electroded so that a suitable voltage can be applied across them. For maximum electromechanical coupling, each ceramic piece is polarized through its thickness. The resulting normal velocity distribution over the surface of each piece is assumed to be reasonably constant. We can stepwise approximate the continuous velocity distribution $u(\theta) = P_\nu(\cos\theta)$ by driving each ceramic piece with a voltage whose magnitude is proportional to the average value of $P_\nu(\cos\theta)$ over its outer surface. Since the desired CBT velocity distribution is rotationally symmetrical, we first subdivide the spherical cap into N bands, with constant θ boundaries. A natural subdivision scheme to use is one with equal angular-width bands. Numerical calculations show that subdivision into ten bands of equal angular width results in excellent constant beamwidth behavior over a large frequency range extending from the low-cutoff frequency f_c for the continuous velocity distribution to an upper frequency limit f_u that depends on the size of the bands. Alternatively, we can subdivide the cap into N bands of equal area. We determined that eight equal area bands are sufficient to produce constant beamwidth behavior, although the top two bands are so much wider than the lower six bands that they probably require further subdivision to suppress possible lateral plate modes in the ceramic. Because of the need to suppress lateral plate modes, we recommend that the CBT be subdivided into at least ten bands whose angular widths are reasonably close to being equal. However, if lateral plate modes are not a problem, any subdivision scheme is acceptable as long as there are at least eight bands, none of which possesses both an angular width greater than $0.1\ \alpha_\nu$ and an area greater than 0.125 times the area of the cap.

A CBT with a stepped velocity distribution possesses an upper frequency limit because the center of the farfield pattern for the acoustic radiation from a single uniformly vibrating band on a sphere exhibits interference maxima and minima as a function of frequency. These extrema occur when the projected height of the band along the axis of the cap; i.e., along the z or polar axis in spherical coordinates, equals an integral number of half-wavelengths, $m\lambda/2$. Odd values of m correspond to maxima and even values correspond to minima. A discussion of this effect is given in Ref. 1, although it was erroneously stated there that odd values of m correspond to minima and even values correspond to maxima.

Thus, the central part of the radiation pattern for a CBT consisting of N uniformly shaded bands may differ substantially from the desired constant beamwidth pattern when the frequency is high enough for one or more of the individual bands to exhibit interference extrema. The band with the largest projected height, which is also the band with the largest area, has the lowest extrema frequency. A conservative rule of thumb for the upper frequency limit f_u is 1.5 times the frequency of the first maximum ($m = 1$) for the band of largest area, excluding those bands for which the value of $P_\nu(\cos\theta)$ is less than about 0.2. We can express this rule of thumb mathematically by

$$f_u = 0.018\,\alpha_\nu^2 f_c/[(\alpha_\nu + 47.7)(\cos\theta_L - \cos\theta_U)], \qquad (26)$$

where f_u and f_c are in the same units, the cap half-angle α_ν is expressed in degrees, and θ_L and θ_U are the lower and upper angular limits of the relevant band.

The interference effects described above are predicted on an ideal geometry and a uniform velocity distribution across each band. The extrema might not be very pronounced in the real world of nonideal geometries and nonuniform velocity distributions. In this case, the transducer could possess good constant beamwidth properties well above the frequency f_u. To be on the safe side, however, we recommend subdivision into as many bands as are required to raise f_u, as calculated from Eq. (26), above the highest desired operating frequency.

A second factor that determines the upper frequency limit is the shape and size of the ceramic pieces used in the mosaic. If the pieces are not identical in shape and size, the upper frequency limit for constancy of both the beam pattern and the transmitting current response is somewhat less than the fundamental resonance of the largest piece. On the other hand, if truly identical pieces can somehow be obtained, they will respond identically with frequency since the acoustic loading is uniform over the entire spherical cap. In this case, the occurrence of a resonance will affect the surface normal velocity magnitude but not its distribution and, thus, the beam pattern will remain constant. Of course, the transmitting current response will follow the frequency dependence of the velocity magnitude, increasing somewhat as the fundamental resonance is approached and decreasing rapidly above resonance. This rapid decrease in response above resonance places a practical upper frequency limit on the CBT.

A third factor that provides an upper frequency limit for a CBT occurs when the outer cap surface is not completely covered with ceramic. In this case, grating-type secondary lobes in the beam pattern can be produced by interference between the individual ceramic pieces in each band. These undesired lobes begin to occur when the spacing between the individual pieces approaches a half wavelength. This effect will be seen in the experimental results presented in Sec. IV for our prototype CBT which contains circular ceramic pieces.

When the CBT consists of a closely packed array of N bands, each band is then driven with a voltage E_i, $i = 1,2,\ldots,$

N, that is proportional to the average of the velocity distribution over the ith band; i.e.,

$$E_i = B\,\langle P_\nu(\cos\theta)\rangle_i = \frac{2\pi B}{A_i}\int_{\theta_{Li}}^{\theta_{Ui}} P_\nu(\cos\theta)\sin\theta\,d\theta, \qquad (27)$$

where θ_{Ui} and θ_{Li} are the upper and lower bounds on θ for the ith band, B is the constant of proportionality, and $\langle\ \rangle_i$ denotes the average over the ith band. The quantity A_i is the solid angle subtended by the ith band and is equal to $2\pi(\cos\theta_{Li} - \cos\theta_{Ui})$.

We can evaluate this integral exactly to give

$$E_i = B\left(\frac{P_{\nu+1}(\cos\theta_{Li}) - \cos\theta_{Li}P_\nu(\cos\theta_{Li}) - P_{\nu+1}(\cos\theta_{Ui}) + \cos\theta_{Ui}P_\nu(\cos\theta_{Ui})}{\nu(\cos\theta_{Li} - \cos\theta_{Ui})}\right). \qquad (28)$$

Numerical tables of Legendre functions of noninteger order are not readily available. Therefore, we express E_i in a trigonometric series by substituting into Eq. (27) the hypergeometric expansion of $P_\nu(\cos\theta)$ in terms of $(1-\cos\theta)/2$ and integrating term by term. This gives

$$E_i = \frac{B}{\cos\theta_{Li} - \cos\theta_{Ui}}\sum_{r=0}^{\infty}\frac{(-1)^r\Gamma(\nu+r+1)}{r!(r+1)!\Gamma(\nu-r+1)2^r}\left[(1-\cos\theta_{Ui})^{r+1} - (1-\cos\theta_{Li})^{r+1}\right], \qquad (29)$$

where the ratio of gamma functions $\Gamma(\nu+r+1)/\Gamma(\nu-r+1)$ equals unity for $r=0$ and equals the following finite product otherwise:

$$\Gamma(\nu+r+1)/\Gamma(\nu-r+1) = (\nu-r+1)(\nu-r+2)\ldots(\nu+r), \quad r\neq 0. \qquad (30)$$

It is seen from Eq. (30) that the ratio of gamma functions equals zero when ν is an integer and $r>\nu$. In this case the Legendre function $P_\nu(\cos\theta)$ is a polynomial of order ν so that its integral and thus the series of Eq. (29) is a polynomial of order $\nu+1$. For ν unequal to an integer the series converges rapidly since $\cos\theta_{Li}$ and $\cos\theta_{Ui}$ are usually quite close to each other and to unity. Convergence to four decimal digits rarely requires more than six or seven terms in the series. There are no approximations involved in Eq. (29); therefore, the error in E_i can be reduced to any desired value by taking enough terms in the series. However, extreme accuracy is unnecessary. Theoretical calculations show that inaccuracies in shading much greater than 1.0% are easily tolerated without significant changes in the radiation properties of a CBT.

We assumed above that the entire outer surface of the cap from $\theta=0$ to $\theta=\alpha_\nu$ was covered with N distinct bands of ceramic. To suppress possible lateral mechanical modes in the ceramic, we subdivide each band into a number of sufficiently small pieces whose width (extent in the ϕ direction) and height (extent in the θ direction) are comparable. We then connect all the pieces in each band electrically in parallel. This procedure results in each ceramic piece being driven with a voltage proportional to the average value of $P_\nu(\cos\theta)$ over the band in which it is located instead of the average value over the outer surface of the piece itself.

If the outer cap surface is not entirely covered with ceramic, then the required voltage shading values E_i are obtained by dividing the expressions given above in Eqs. (27) to (29) by the packing fractions F_i to obtain $E_i' = E_i/F_i$. The packing fraction F_i is defined to be that fraction of the area of the ith band that is covered by ceramic. Calculations for CBTs where the cap surface is not entirely covered with ceramic; e.g., when circular elements are used, showed that the constant beamwidth properties are preserved even when the packing fraction is as low as 30%. Of course, as the packing fraction decreases, the frequency at which grating-type lobes begin to occur also decreases thereby reducing the frequency band of operation.

Additional design information for a CBT based on a mosaic of piezoelectric ceramic is given in Ref. 8. Included are expressions for the source level, transmitting voltage and current responses, and receiving voltage sensitivity. We note an error in several of these expressions. The factor F_i should be removed from Eqs. (47)–(49) and (51) since these were derived for a close-packed mosaic with a packing fraction of unity for all bands. The corresponding expressions, when the mosaic is not close packed, can be obtained by inserting the factor F_1 into the numerator of the right-hand side of Eq. (40) and carrying it through the calculations to Eq. (45), retaining F_1 in Eqs. (47) and (48), but still removing F_1 from Eqs. (49) and (51). This assumes that E_1/F_1 is larger than E/F for any other band so that the voltage applied to the CBT is applied unshaded to the first band and reduced by the factors E_iF_1/E_1F_i for each of the other bands. If some other E/F is largest, say for the I th band, then the voltage is applied unshaded to the I th band and reduced by the factors E_iF_I/E_IF_i for each of the other bands. In this case, the equations in Ref. 8 are modified as indicated above except that the factor E_1F_I/E_I is used instead of the factor F_1.

III. PROTOTYPE CBT

We designed and constructed a prototype CBT based on P_5 Legendre function shading for use in the Underwater Sound Reference Detachment's (USRD) Anechoic Tank Facility. A P_5 CBT has a cap half-angle of 25.0° and a theoretical beam pattern with a -3-dB half-angle of about 11.8°, as calculated using Eqs. (2) and (3), respectively. We selected a cap radius of 15.25 cm (radius of curvature equal to 0.349 m). This provides a cutoff frequency for operation in water of 20.9 kHz, as calculated using Eqs. (9).

The spherical cap is an aluminum plate in which 849 circular cavities, 0.805 cm in diameter and 0.623 cm deep, have been machined in a closely spaced pattern consisting of 16 concentric bands surrounding a center cavity. A circular

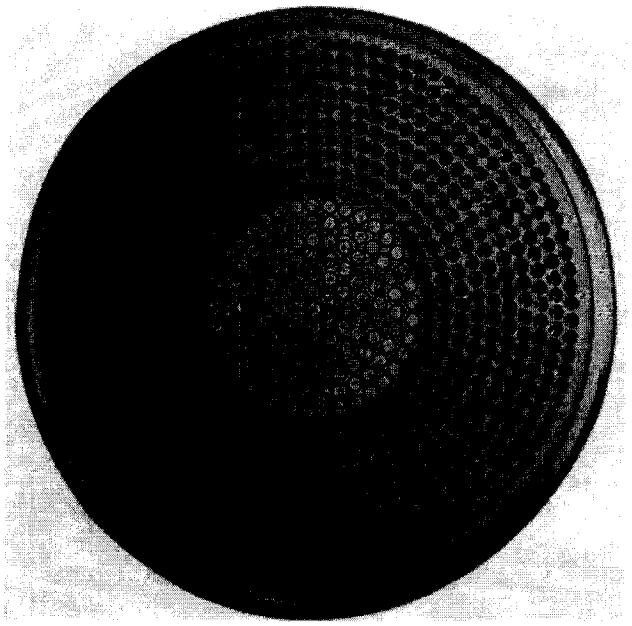

FIG. 7. Front face of the prototype CBT when partially assembled.

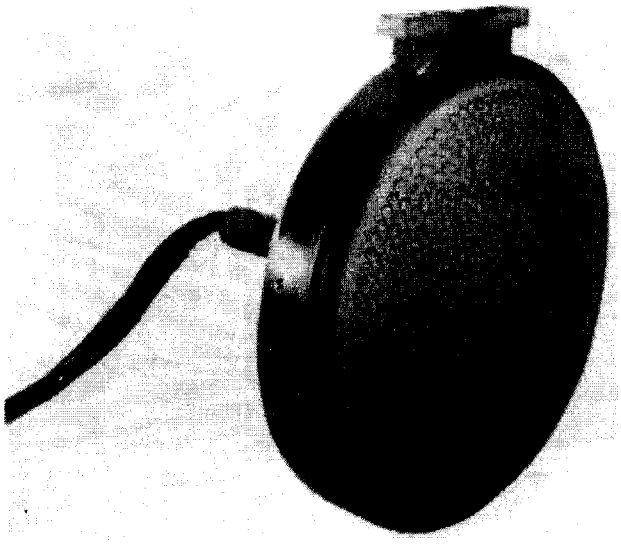

FIG. 8. Prototype constant beamwidth transducer.

disk element, 0.635 cm in diameter and 0.318 cm thick, of lead zirconate–titanate [MIL-STD-1376 (SHIPS) type I piezoelectric ceramic] is inserted into each circular cavity with the front face of the disk flush with the front face of the plate. All of the disks are electroded both front and back and polarized through their thickness. We placed a strip of corprene, 0.085 cm thick, around the edges of each disk and a layer of corprene, 0.305 cm thick, behind each disk in order to mechanically isolate the disks from the aluminum plate.

Figure 7 shows the transducer face during construction with the six inner bands already assembled. After all the bands were assembled, we connected all of the elements in each band in parallel. The center disk is considered to be part of the first band, resulting in seven disks for that band. The common negative lead was obtained by soldering a wire to each of the outer faces of the disks in the band and then passing this wire through a hole with an insulated sleeve to the back of the aluminum plate. During assembly, individual positive leads were attached with conducting epoxy to the back face of each of the disks. These leads were passed through small holes with insulated sleeves to the back of the aluminum plate. The common positive lead was obtained by soldering each of the individual positive leads in the band to a circular wire buss.

When all of the electrodes were in place, the aluminum plate was connected to a stainless steel backing plate designed to provide a watertight air cavity capable of withstanding the hydrostatic pressure (up to 6.9 MPa) encountered in the anechoic tank. A removable part in the center of the backing plate provides access to the cavity. The part contains a high-pressure bulkhead connector for attaching the transducer's electrical cable. An acoustic window 0.32 cm thick was cast over the entire front face to provide water integrity. RHO-C rubber was used in order to minimize potential adverse acoustic effects of the window. The completed transducer is shown in Fig. 8.

IV. EXPERIMENT

We tested the prototype CBT in the Anechoic Tank Facility at frequencies from 10 to 200 kHz and at ambient pressures up to 3.4 MPa. The CBT was operated as a projector although it is equally usable as a receiver.

The band shading was accomplished by placing capacitors in series with each band to form a voltage divider. By measuring the total capacitance of the active elements in a band, the series capacitance required to produce the desired signal voltage across the elements could be calculated. The desired relative voltage levels for the bands were determined by first computing E_i using Eq. (28), dividing by the band packing fractions F_i, and then dividing by the nominal values of the piezoelectric constant d_{33} for each band. The 849 piezoceramic disks had been presorted according to d_{33} values prior to installation in order to obtain high uniformity throughout each band. The shading capacitors were installed in the transducer cavity.

We encountered great difficulty in accurately maintaining the required shading of the bands throughout the desired frequency range. It was determined that the capacitance of the active elements changed significantly as a function of frequency (and temperature). We were unable to find shading capacitors which matched this frequency (and temperature) dependence. This made it necessary to change the shading capacitance at each frequency (and temperature) in order to regain the proper shading. To accomplish this, the internal shading capacitors were removed and an external shading box was constructed.

The shading box consisted of 16 sets of fixed and variable capacitors connected in series with the active elements through 16 coaxial cables. The box permitted monitoring of the signal voltage across the elements in each band and adjustment of the shading capacitance while the transducer was mounted in the anechoic tank. Shading adjustments were required whenever the measurement frequency was changed. No new adjustments were required when the hydrostatic pressure was changed.

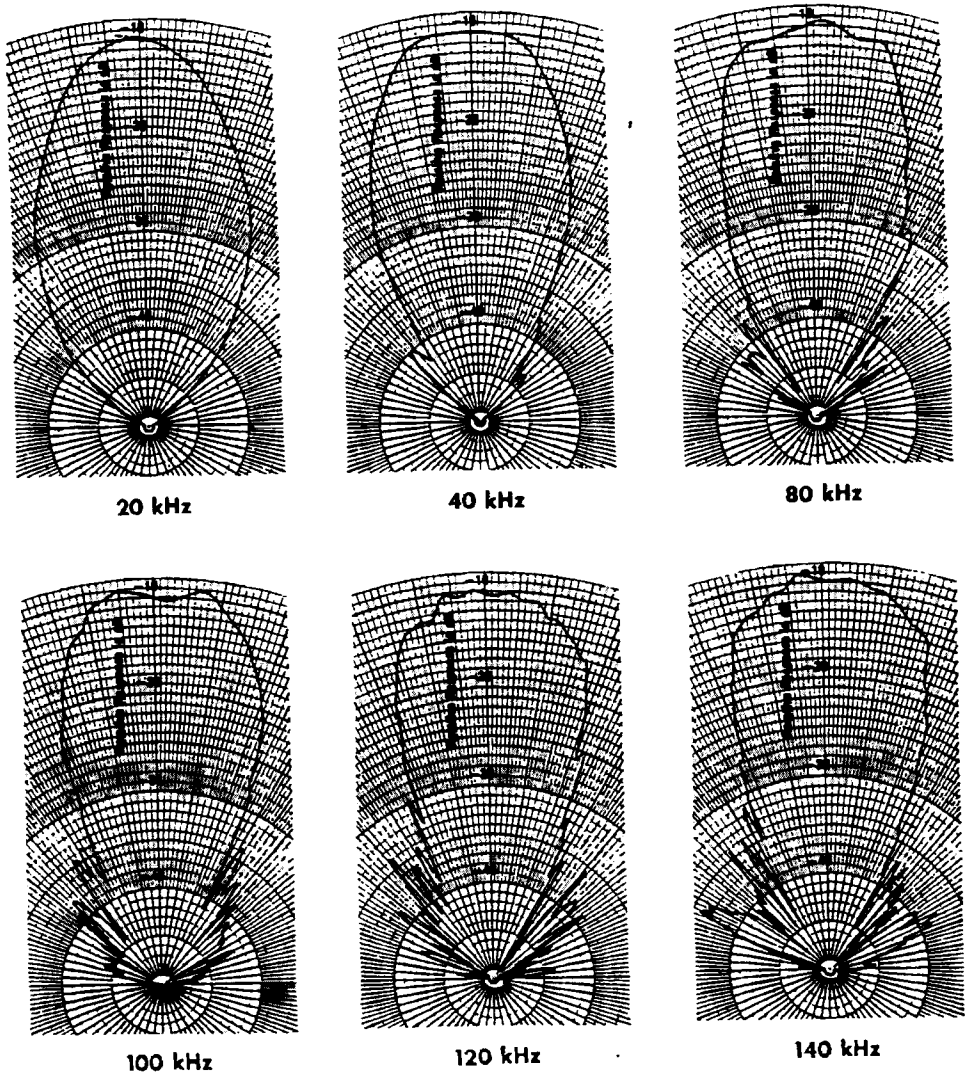

FIG. 9. Beam patterns for prototype CBT at several selected frequencies.

We obtained directivity beam patterns by rotating the CBT and monitoring its transmitted acoustic pressure with a USRD type F50 hydrophone located 2 m away. The beam patterns for several frequencies are shown in Fig. 9. These patterns show a nearly constant beamwidth over the frequency range from 20 to 140 kHz. They also possess very low side lobes throughout this frequency range. As the frequency was increased above 140 kHz, however, the side lobes increased markedly until they were only about 6 dB below the mainlobe at 200 kHz. The patterns were virtually unchanged as the hydrostatic pressure was increased from ambient pressure to 3.4 MPa (corresponding to 340 m of water depth).

The transmitting current response for the prototype CBT is shown in Fig. 10. The measured results are indicated by the solid curve while the corresponding theoretical values are given by the dashed curve. We obtained the theoretical values by computer calculations based on measured dielectric and piezoelectric properties of the individual circular disk elements used in the CBT. At low frequencies the measured results are uniformly about 4 dB below theoretical predictions. This difference is probably attributable to the presence of a large amount of corprene on the radiating surface of the transducer; over 21% of the area is covered with corprene. The corprene has a relatively high compliance compared with water and tends to "short circuit" a significant fraction of the volume velocity produced by the motion of the circular disks. A resulting reduction in the radiated acoustic pressure of several decibels is not surprising. The valley in the theoretical curve near 140 kHz is due to a local minimum in the individual element capacitance. Theoretical results obtained for a close-packed array of ideal elements

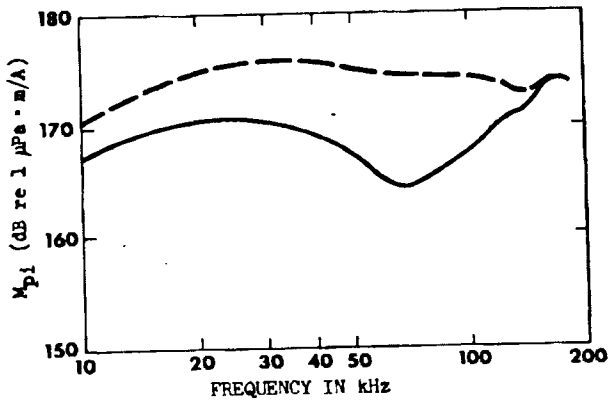

FIG. 10. Transmitting current response of the prototype CBT. Measured results are indicated by the solid curve, theoretical values by dashed curve.

show a virtually flat transmitting current response above about 60 kHz.

The difference between theory and experiment increases and then decreases as the frequency increases above 35 kHz due to the effect of a broad resonance at about 180 kHz. This resonance is probably mechanical since it is well below the lowest resonance frequency of about 290 kHz noticeable in the input electrical impedance of a single circular disk element. Even with an unwanted resonance present, the transmitting current response varies by less than 6 dB over the broad frequency range from 10 to 120 kHz. It is important to note that the prototype design was selected to minimize construction costs and is in no way optimum; for example, the use of corprene will be significantly reduced in future designs.

V. SUMMARY AND CONCLUSIONS

We have presented design formulas for a constant beamwidth transducer based on Legendre function amplitude shading of a spherical cap. Included are simple algebraic and trigonometric expressions for the required velocity distribution, beam patterns, directivity index, equivalent two-way beamwidths for volume and surface reverberation, spherical cap size, and shading coefficients for a stepwise implementation of the velocity distribution. Most of the expressions are extremely accurate approximations for difficult-to-evaluate expressions in terms of Legendre functions of fractional order.

We designed and constructed a prototype CBT based on P_5 shading. The measured directivity patterns possessed very low side lobes and a nearly constant beamwidth over the frequency range from 20 to 140 kHz and for ambient pressures up to 3.4 MPa. The results show that, with the proper design and shading, a transducer can be constructed which has a relatively constant beamwidth over a large frequency range. The only significant problem remaining is maintaining the shading throughout the desired frequency range. It is believed that this problem can be solved by installing a separate amplifier for each band of active elements. Power amplifiers would be used if a projector were desired or preamplifiers for a receiver. These amplifiers could be installed inside the transducer housing. The shading could be accomplished by adjusting the gain of each amplifier. This would decouple the shading from changes in the capacitance of the active elements. A single transducer could function as both a projector and a receiver by installing both types of amplifiers and employing remote switching to select the proper type.

ACKNOWLEDGMENTS

The authors gratefully acknowledge the contributions of Gary Gallagher to the construction of both the CBT and the shading box. We would also like to thank Robert Dalton for his precision machining of the CBT components and Clementina Ruggiero for the computer program used in performing this machining. This work was performed in the Acoustic Metrology Program sponsored by the Naval Sea Systems Command (SEA63R12).

[1]P. H. Rogers and A. L. Van Buren, "New Approach to a Constant Beamwidth Transducer," J. Acoust. Soc. Am. **64**, 38–43 (1978).
[2]W. J. Trott, "Design Theory for A Constant-Beamwidth Transducer," NRL Rep. No. 7933 (1975).
[3]M. Abramowitz and I. A. Stegun, *Handbook of Mathematical Functions*, NBS Applied Mathematics Series No. 55, Washington, DC (1965), p. 369.
[4]E. Jahnke and F. Emde, *Tables of Functions with Formulae and Curves* (Dover, New York, 1945), 4th ed., p. 156.
[5]Harvard Computation Laboratory, *Tables of the Bessel Functions of the First Kind of Orders Zero and One*, Vol. 3 (Harvard U. P., Cambridge, MA, 1947).
[6]R. J. Urick, *Principles of Underwater Sound* (McGraw–Hill, New York, 1975), 2nd ed., p. 217.
[7]J. L. Butler and S. L. Ehrlich, "Superdirective Spherical Radiator," J. Acoust. Soc. Am. **61**, 1427 (1977).
[8]A. L. Van Buren, "Design Manual for a Constant Beamwidth Transducer," NRL Rep. No. 8329 (1979).